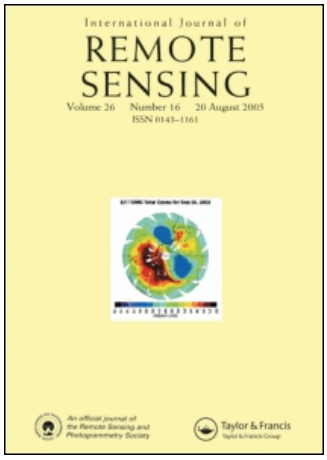

International Journal of Remote Sensing
Publication details, including instructions for authors and subscription information:
http://www.informaworld.com/smpp/title~content=t713722504

In-flight calibration of NOAA AVHRR visible and near-IR bands over Greenland and Antarctica

N. G. Loeb

Online Publication Date: 01 February 1997
To cite this Article: Loeb, N. G. (1997) 'In-flight calibration of NOAA AVHRR visible and near-IR bands over Greenland and Antarctica', International Journal of Remote Sensing, 18:3, 477 - 490
To link to this article: DOI: 10.1080/014311697218908
URL: http://dx.doi.org/10.1080/014311697218908

INT. J. REMOTE SENSING, 1997, VOL. 18, NO. 3, 477–490

In-flight calibration of NOAA AVHRR visible and near-IR bands over Greenland and Antarctica

N. G. LOEB

College of Oceanic and Atmospheric Sciences, Oregon State University, Rm. 326 Strand Agriculture Hall, Corvallis, OR 97331-2209, U.S.A.

(*Received 7 May 1996; in final form 1 August 1996*)

Abstract. A new method for in-flight calibration of NOAA AVHRR visible and near-IR bands is presented. The approach involves using calibrated NOAA-9 near-nadir reflectances over spatially and temporally uniform ice-surfaces from Greenland and Antarctica to produce reflectance calibration curves for AVHRR instruments in all orbits. The reflectance calibration curves consist of second order polynomial regressions of reflectance on solar zenith angle, derived from observations that are spatially uniform in all AVHRR channels over sub-regions of area 68 km by 68 km. By comparing reflectances from uncalibrated AVHRR instruments with these calibration curves, new channel 1 and 2 calibration coefficients are obtained with an accuracy of ≈5 per cent. The main advantages of this calibration method are: (1) calibration targets are large; (2) it can be applied over multiple years; (3) it is applicable for a wide range of solar zenith angles, and can therefore be used year-round. When calibration coefficients inferred from NOAA-11 (1994) and NOAA-14 (1995) observations over Greenland and Antarctica are compared with those from the formulae of Rao and Chen (1995, 1996), the two methods are in excellent agreement in channel 1 (within ≈3 per cent). In channel 2, they agree to within ≈4 per cent for NOAA-14, but are significantly different for NOAA-11 (≈9 per cent). When applied to NOAA-12 AVHRR observations for 1994–95, channel 1 and 2 calibration coefficients are ≈20 per cent and ≈35 per cent larger than prelaunch values, respectively.

1. Introduction

In order to obtain quantitative information from satellite measurements, the satellite radiometer must first be calibrated. Calibration is crucial in applications which use theoretical/empirical retrieval methods to infer physical variables from measurements. For instruments such as the NOAA Advanced Very High Resolution Radiometer (AVHRR), this is a problem since absolute calibration of channel 1 (wavelength 0·64 μm) and channel 2 (wavelength 0·83 μm) is only available prior to satellite launch. Instrument calibration changes in time due to outgassing, launch-associated stresses (such as vibrations and exhaust contamination), and exposure to the harsh space environment (Rao and Chen 1995). Several investigators (Whitlock *et al.* 1990, Staylor 1990, Rao and Chen 1995, Teillet *et al.* 1990) have conducted post-launch calibration of the AVHRR channels by matching near-simultaneous satellite scan spots with calibrated ground and aircraft measurements over desert surfaces. This approach has limitations, however, since it is costly, requires considerable effort, and cannot be used to calibrate historical data.

Recognizing these problems, Kaufman and Holben (1993) proposed two methods for in-flight calibration of NOAA AVHRR. The first, over ocean, relies on

comparisons between theoretical calculations and observations in the backscattering direction and in the Sun glint region; the second involves the use of large homogeneous fixed desert targets ($\approx$100 km^2) as calibration sources. While the desert method is more accurate, it is nonetheless sensitive to spatial and temporal variations in aerosol and water vapor amount, clouds and dust outbreaks, and variations in the view and solar zenith angle across the calibration site.

Here a new method for in-flight calibration of the AVHRR visible and near-infrared channels involving observations over the permanent ice-sheets of Greenland and Antarctica is presented. The underlying assumption is the same as that over deserts, namely, that the reflectivity of the surface-atmosphere system is stable—both spatially and temporally. From calibrated NOAA-9 AVHRR reflectances over uniform ice-covered regions, reflectance calibration curves are derived for calibrating AVHRR instruments in other orbits (e.g., NOAA-11, NOAA-12 and NOAA-14). The calibration curves consist of second order polynomial regressions of near-nadir reflectance on solar zenith angle. By comparing reflectances from an uncalibrated instrument with the calibration curves, new channel 1 and channel 2 calibration coefficients are inferred.

The advantages of using calibration targets over Greenland and Antarctica are: (1) these targets are very large; (2) they are permanent (allowing calibration over multiple years); (3) frequent satellite passes over these regions makes the calibration more flexible (in fact, reflectance calibration curves are provided for a wide range of solar zenith angles); (4) ground-based measurements are not required.

In the following, a description of how the reflectance calibration curves are constructed and how they can be used is provided. The technique is then directly compared with that of Rao and Chen (1995, 1996) using observations from AVHRR NOAA-11 (June 1994) and NOAA-14 (June and December 1995). Finally, calibration of the 0·64 and 0·83 μm NOAA-12 AVHRR channels over the period from June 1994 to December 1995 is provided.

2. Observations

For a given raw pixel count C in channel i, the reflectance (or equivalently, the isotropic albedo) R_i (in per cent) at the mean Sun-Earth distance is determined from the channel calibration coefficient α_i and offset β_i provided as part of the AVHRR Level 1B data as follows:

$$R_i = \frac{(\alpha_i C + \beta_i)\varepsilon_{se}}{\mu_0} \tag{1}$$

where μ_0 is the cosine of the solar zenith angle θ_0, and $\varepsilon_{se} = (\delta_s/\bar{\delta}_s)^2$ is a correction which normalizes observed reflectances (at a given Sun-Earth separation δ_s) to the mean Sun-Earth distance $\bar{\delta}_s$. C is related to the pixel radiance I_i (in W m^{-2} sr^{-1} μm^{-1}) through:

$$I_i = (a_i C + b_i)\varepsilon_{se} \tag{2}$$

where

$$a_i = \alpha_i \left(\frac{F_i}{100\pi w_i}\right) \tag{3}$$

$$b_i = \beta_i \left(\frac{F_i}{100\pi w_i}\right) \tag{4}$$

F_i (in $W\,m^{-2}$) is the integrated solar irradiance weighted by the spectral response function of the channel, and w_i (in μm^{-1}) is the equivalent width of the spectral response function (Kidwell 1994).

Global Area Coverage (GAC) measurements from NOAA-9, NOAA-11, NOAA-12 and NOAA-14 over Greenland and Antarctica are considered. GAC AVHRR data is produced by sampling AVHRR 1 km data to 4 km resolution by averaging along-scan groups of four samples out of five and using every third scan (Kidwell 1994). The observations over Antarctica and Greenland are subdivided into images consisting of 512 scan lines by 408 pixels across-track. Table 1 shows the number of images considered for each of the NOAA AVHRR instruments. To reduce uncertainties caused by view angle dependencies, and by variations in surface type, only pixels with view angles $<18°$ are considered, and only pixels lying well within the interiors of Greenland and Antarctica (i.e., away from the coastlines) are included. The uncertainty due to changes in the anisotropy of the reflectance over this interval is estimated to be $\approx$1 per cent based on a sensitivity analysis of measurements stratified by view and relative azimuth angle.

For the AVHRR instruments listed in table 1, post-launch calibration is available for NOAA-9 and NOAA-11 from Rao and Chen (1995), and for NOAA-14 from Rao and Chen (1996). These studies provide formulae of calibrated channel 1 and 2 radiances (and therefore a_i and α_i) in terms of elapsed time in orbit, expressed in terms of the number of days following the satellite launch. The NOAA-9 formulae for the period of 1985–86 are likely the most reliable of these since they are based on the most extensive set of aircraft/satellite measurements (e.g., Smith *et al.* 1988, Whitlock *et al.* 1990, Rao and Chen 1995). In fact, NOAA-9 AVHRR was used by Rao and Chen (1995) as a normalization standard to establish relations between AVHRR radiances from NOAA-7 and NOAA-11. Extrapolation of the Rao and Chen (1995) formulae for NOAA-11 to June, 1994 is probably less reliable, however, since the degradation rates in these formulae are based on measurements obtained prior to 1992. In contrast, more recent data (after 1994) was used by Rao and Chen (1996) for the NOAA-14 AVHRR formulae.

3. Methodology

Ideally, calibration of satellite radiometers requires targets whose reflectances are stable, both spatially and temporally, over large homogeneous areas. Over Greenland

Table 1. Number of images over Greenland and Antarctica for each of the NOAA AVHRR instruments considered in this study.

Month/year	Region	Satellite	No. of images
June 1985	Greenland	NOAA-9	20
December 1985	Antarctica	NOAA-9	22
June 1986	Greenland	NOAA-9	17
December 1986	Antarctica	NOAA-9	12
June 1994	Greenland	NOAA-11	14
June 1994	Greenland	NOAA-12	13
December 1994	Antarctica	NOAA-12	10
June 1995	Greenland	NOAA-12	10
June 1995	Greenland	NOAA-14	13
December 1995	Antarctica	NOAA-12	9
December 1995	Antarctica	NOAA-14	17

and Antarctica, the temporal constraint is likely well satisfied since the ice-sheets are permanent and remote from any sources of pollution. The spatial homogeneity requirement is more of a problem since, at any given time, cloud cover may be present. At the pixel level, identification of cloud over an ice covered area can be extremely difficult since clouds can have similar reflective and thermal properties as ice at AVHRR wavelengths. A more effective approach is to consider the spatial distribution of reflectances and brightness temperatures over regions that are large compared to the pixel resolution. Here the GAC AVHRR images are divided into sub-regions of 17 pixel by 17 pixel arrays (68 km × 68 km). For each sub-region, an index of homogeneity is calculated from the following:

$$N = \frac{1}{4}\left(\frac{\sigma_1}{R_1} + \frac{\sigma_2}{R_2} + \frac{\sigma_3}{T_3} + \frac{\sigma_4}{T_4}\right) 25\% \tag{5}$$

where σ_i is the standard deviation of the reflectances or brightness temperatures in the i_{th} channel, $\bar{R}_1$ and $\bar{R}_2$ are the mean reflectances in channels 1 and 2, and $\bar{T}_3$ and $\bar{T}_4$ are the mean brightness temperatures in channels 3 (3·7 μm) and 4 (11 μm). Small N means the sub-region is spatially homogeneous in the visible and infrared; large N implies that pixel reflectances and/or brightness temperatures within the sub-region are very different.

Figure 1 (*a*) and (*b*) show scatterplots of calibrated (based on Rao and Chen 1995) NOAA-9 AVHRR near-nadir reflectances in channels 1 and 2 as a function of N for scenes over Antarctica (December 1985) with solar zenith angles θ_0 between 63° and 68°. When N is small, reflectances appear quite stable—the scatter about the mean is less than ≈2 per cent. As N increases, the scatter becomes much larger, and many samples fall well below values obtained at small N. This increase in scatter is likely associated with the presence of cloud over the sub-region. At low Sun elevations, radiative transfer calculations show a tendency for nadir reflectances to decrease at visible wavelengths when a cloud layer (regardless of thickness) is inserted above a highly reflecting ice surface. Under these conditions, the cloud layer tends to re-direct much of the incident solar radiation into the forward scattering direction at oblique viewing angles, causing a reduction in the amount of radiation which can be reflected into the nadir direction from the highly reflecting ice surface. Another factor which may explain the reduced reflectivities is cloud shadowing—shadows cast by clouds on the surface tend to lower reflectivities.

Based on figure 1, it is assumed that sub-regions with $N < 0{\cdot}75$ per cent are stable and representative of reflectances over cloud-free uniform ice-surfaces. Figures 2 (*a*) to (*d*) show calibrated NOAA-9 channel 1 and 2 reflectances for all sub-regions within the interiors of Greenland and Antarctica which satisfy this condition. The gap in figures 2 (*c*) and (*d*) between $\theta_0 = 57°$–$64°$ occurs because only two orbits per day were available for NOAA-9. The cluster between $\theta_0 = 46°$–$57°$ corresponds to the ascending orbit while the second cluster at lower Sun corresponds to the descending orbit. In all cases, reflectances decrease smoothly with increasing solar zenith angle, differences between the 1985 and 1986 results are small, and no systematic behaviour in the differences is observed. That such a smooth reflectance dependence on solar zenith exists over areas as vast as the interiors of Greenland and Antarctica is a clear indication that these regions are spatially uniform. Factors affecting this result, such as undetected cloud and changes in surface characteristics, have only a minor influence when the $N < 0{\cdot}75$ per cent constraint is applied. The remarkable

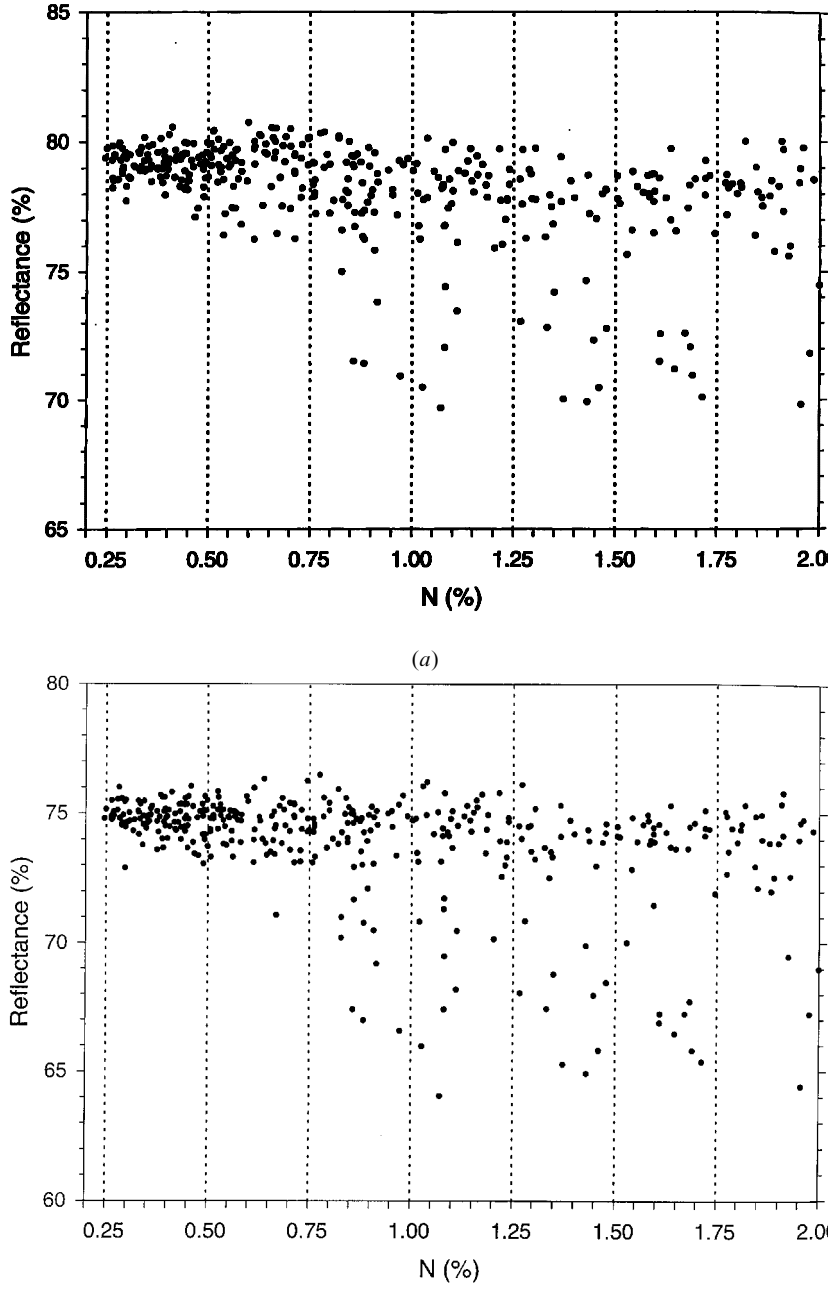

Figure 1. NOAA-9 AVHRR near-nadir reflectance vs N over Antarctica (December 1985) for solar zenith angles between 63° and 68° in (*a*) channel 1 and (*b*) channel 2.

similarity between the 1985 and 1986 reflectances clearly demonstrates that these regions are also temporally stable, so that calibration over multiple-years is possible.

The solid lines in figure 2 are least-squares second order polynomial fits of the

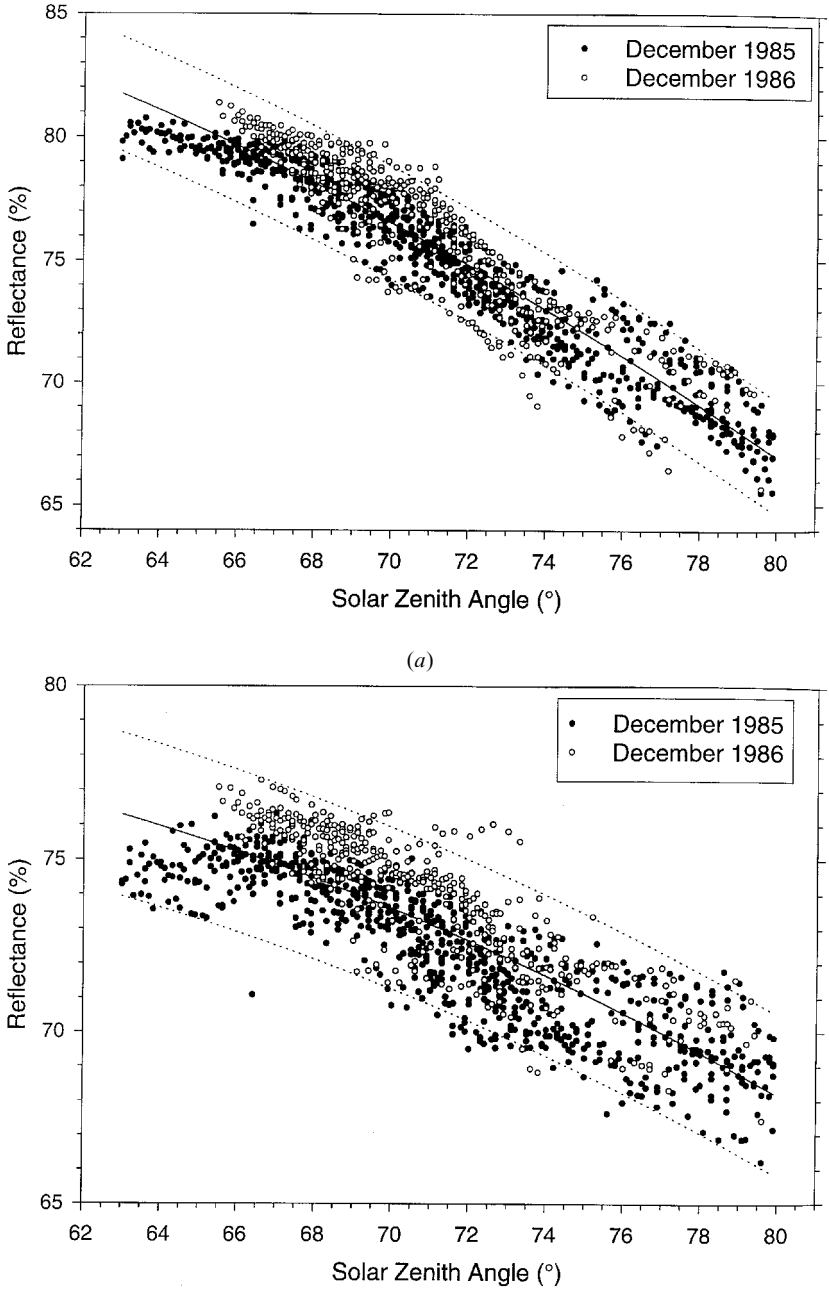

(*a*)

(*b*)

Figure 2. NOAA-9 AVHRR near-nadir reflectance vs solar zenith angle for $N<0{\cdot}75\%$ in (*a*) channel 1 (Antarctica, December 1985–86); (*b*) channel 2 (Antarctica, December 1985–86); (*c*) channel 1 (Greenland, June 1985–86); (*d*) channel 2 (Greenland, June 1985–86). Dashed lines represent 95% prediction intervals.

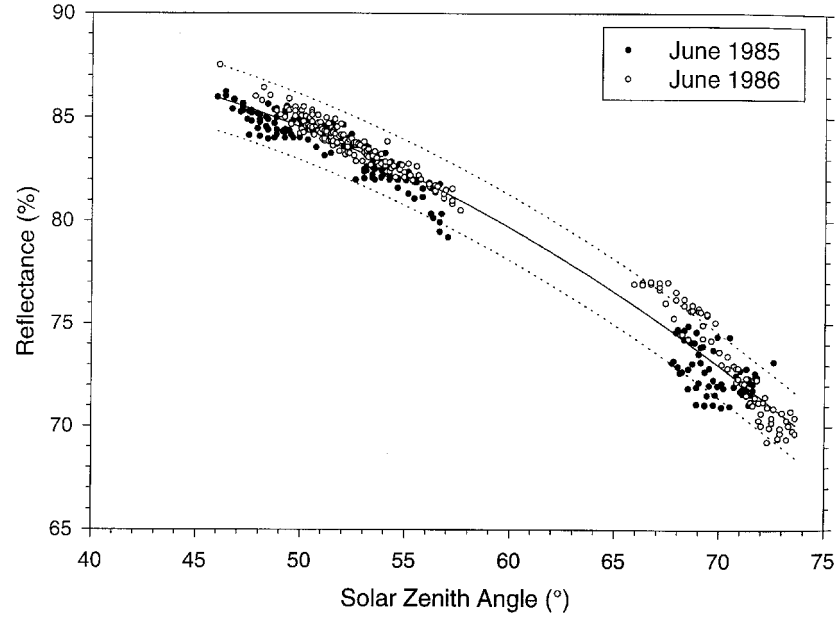

(*c*)

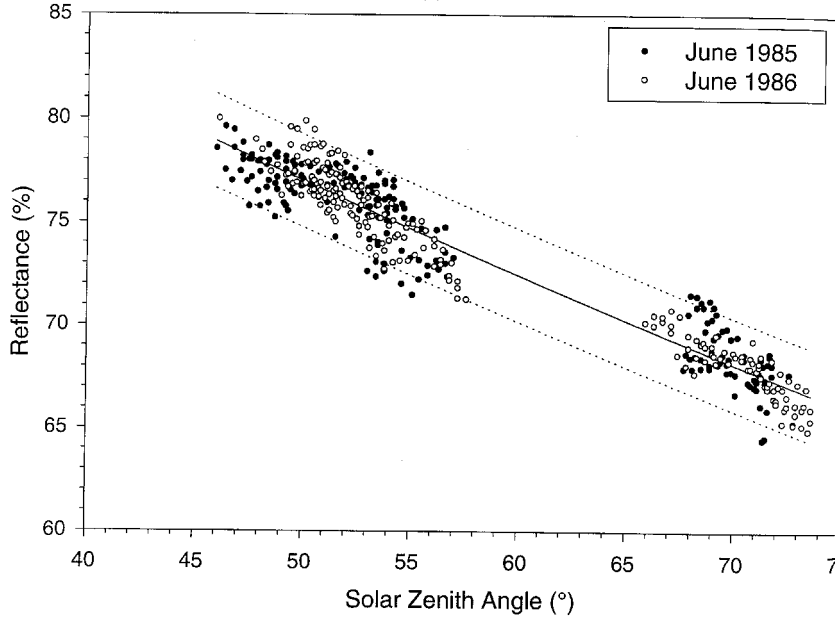

(*d*)

form:

$$R = c_2\theta_0^2 + c_1\theta_0 + c_0 \tag{6}$$

where the regression coefficients c_0, c_1, c_2 are provided in table 2. Uncertainties in the regressions are estimated using 95 per cent prediction intervals, indicated by the

Table 2. Regression coefficients for reflectance calibration curves constructed from calibrated NOAA-9 AVHRR reflectances in channels 1 and 2 ($R = c_2\theta_0^2 + c_1\theta_0 + c_0$).

	Channel 1			Channel 2			
Region	c_0	c_1	c_2	c_0	c_1	c_2	θ_0 range
Greenland	81·37	0·5202	−0·009152	103·9	−0·6072	0·001373	46°–73°
Antarctica	74·25	0·8953	−0·01233	60·29	0·8305	−0·009150	63°–80°

dashed lines. These regression curves are used as a reference in calibrating AVHRR in orbits other than that of NOAA-9. By comparing reflectances from uncalibrated AVHRR instruments with those from the NOAA-9 calibration curves, new calibration coefficients are derived. Given a pixel count C at θ_0 from an uncalibrated instrument, a new calibration coefficient α_i' is inferred from the following:

$$\alpha_i' = \frac{\mu_0 R_i'(\mu_0)/\varepsilon_{se} - \beta_i}{C} \tag{7}$$

where $R_i'(\mu_0)$ is determined from the NOAA-9 reflectance calibration curves in figure 2. β_i is assumed to remain constant in equation (7). A quantity useful for comparison purposes is the calibration ratio, defined as $\gamma_i = \alpha_i/\alpha_i'$ (Kaufman and Holben 1993).

The uncertainty in α_i' over a given sub-region is calculated based on equation (7) by assuming an uncertainty in R_i' of $\pm 2{\cdot}5$ per cent (absolute reflectance). This uncertainty in R_i' is inferred from the 95 per cent prediction intervals in figures 2(*a*) and (*b*). The main causes for uncertainties in R_i' (or α_i') are likely associated with the presence of undetected cloud, and temporal and spatial variations in surface reflectance properties over Greenland and Antarctica. In the latter case, measurements in channel 1 will tend to be more sensitive to the presence of small amounts of absorbing impurities in the surface (Warren and Wiscombe 1980), while channel 2 reflectances will tend to be sensitive to changes in snow grain size (Wiscombe and Warren 1980). Other sources of uncertainty include those due to changes in the anisotropy of the reflectance over ice for viewing angles in the 0°–18° range (<1 per cent), variations in atmospheric properties such as ozone, aerosol and water vapour amounts, and instrument polarization effects.

4. Results

Figures 3(*a*) and (*b*) and table 3 summarize the calibration results for NOAA-11 during June, 1994 obtained in the present study and from the Rao and Chen (1995) formulae. Figures 4 and 5 and table 4 provide similar results but for NOAA-14 during June and December, 1995. Overall, the two methods are in excellent agreement in channel 1. In all cases, relative differences in α_i' are <3 per cent which is less than the uncertainty (≈5 per cent). In channel 2, while the two methods agree for NOAA-14 (relative differences <4 per cent), significant differences are observed for NOAA-11—calibration coefficients inferred from Rao and Chen (1995) are ≈9 per cent higher (relative difference). The larger discrepancy for NOAA-11 may in part be because, as noted earlier, degradation rates used in the NOAA-11 formulae of Rao and Chen (1995) were derived from measurements obtained prior to 1992.

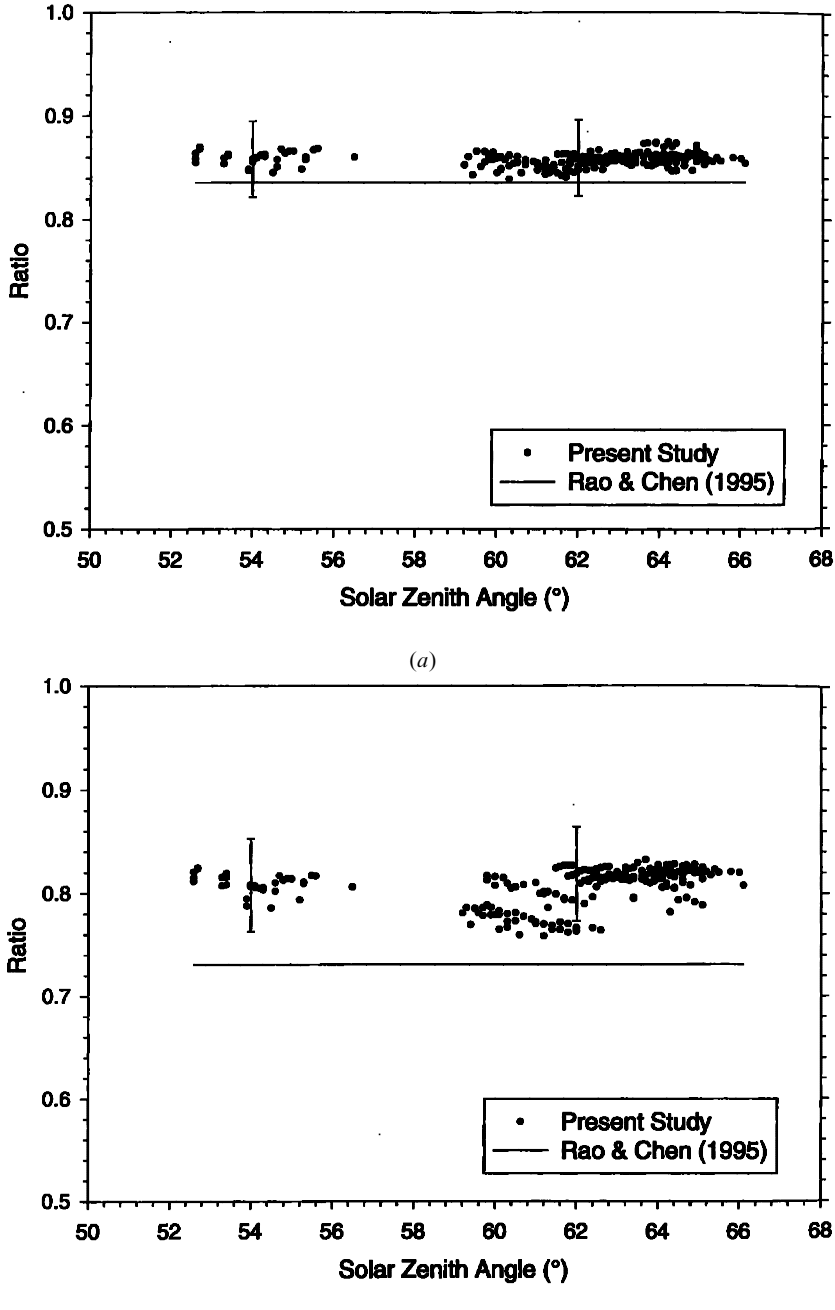

Figure 3. NOAA-11 ratios in (*a*) channel 1 and (*b*) channel 2 for June 1994, using the procedure described in this study and from the formulae of Rao and Chen (1995). The error bar length is representative of the uncertainty in the ratio estimates.

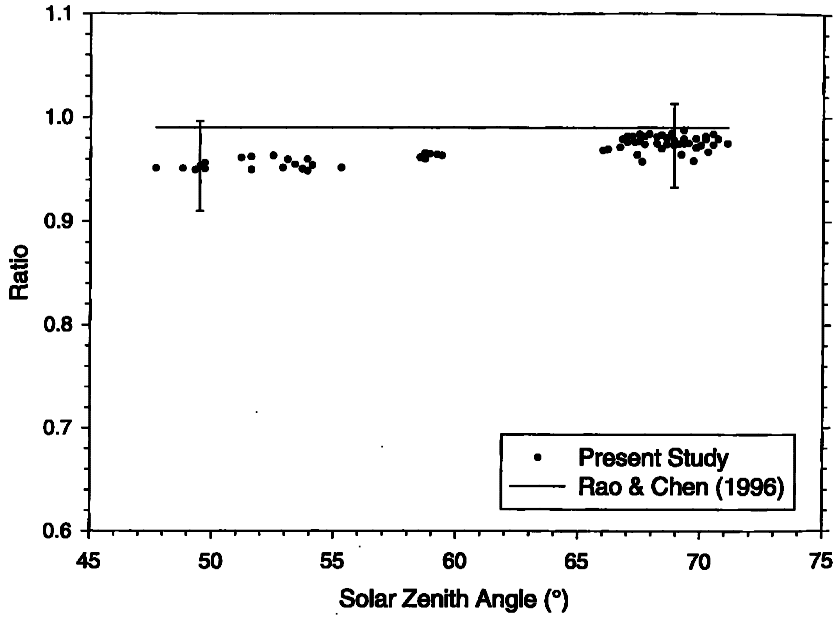

(*a*)

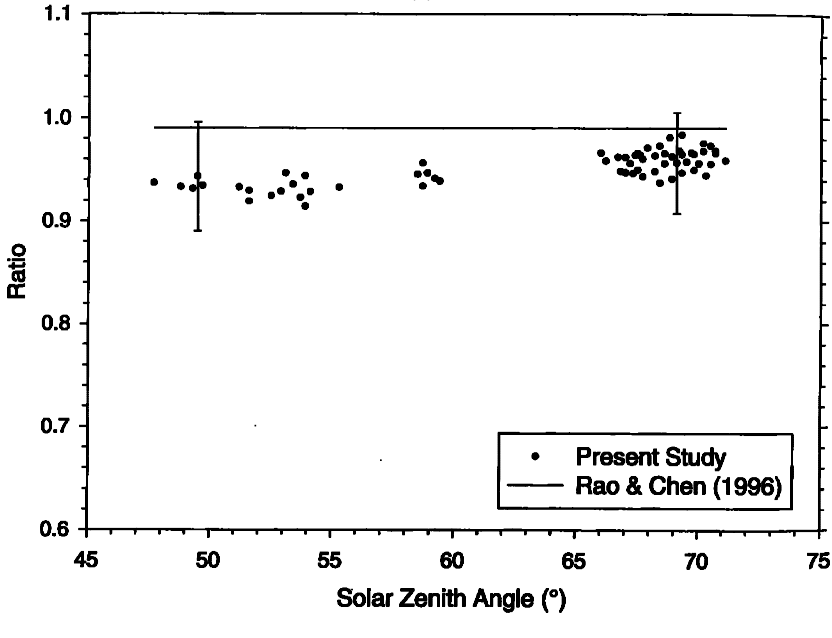

(*b*)

Figure 4. NOAA-14 ratios in (*a*) channel 1 (Greenland, June 1995); (*b*) channel 2 (Greenland, June 1995); (*c*) channel 1 (Antarctica, December 1995); (*d*) channel 2 (Antarctica, December 1995) using the procedure described in this study and from the formulae of Rao and Chen (1996). The error bar length is representative of the uncertainty in the ratio estimates.

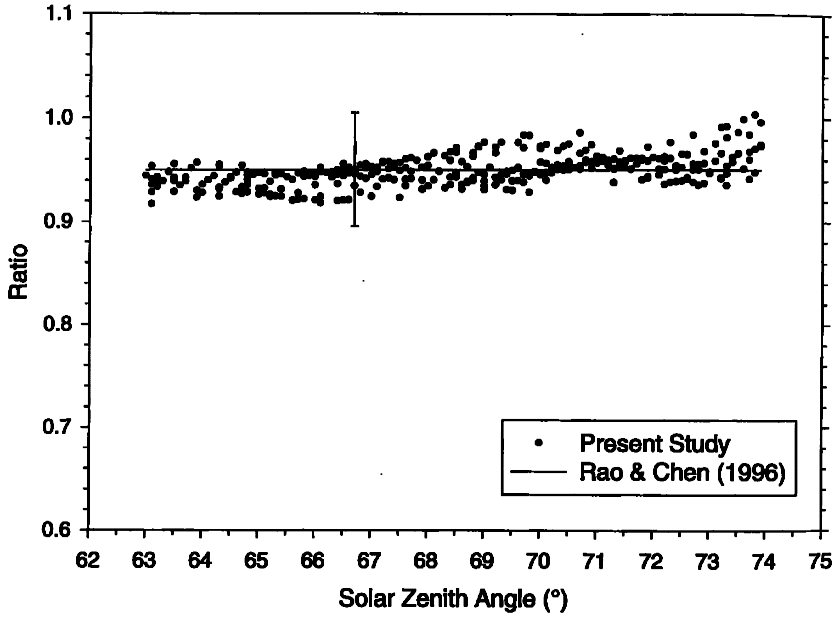

(*c*)

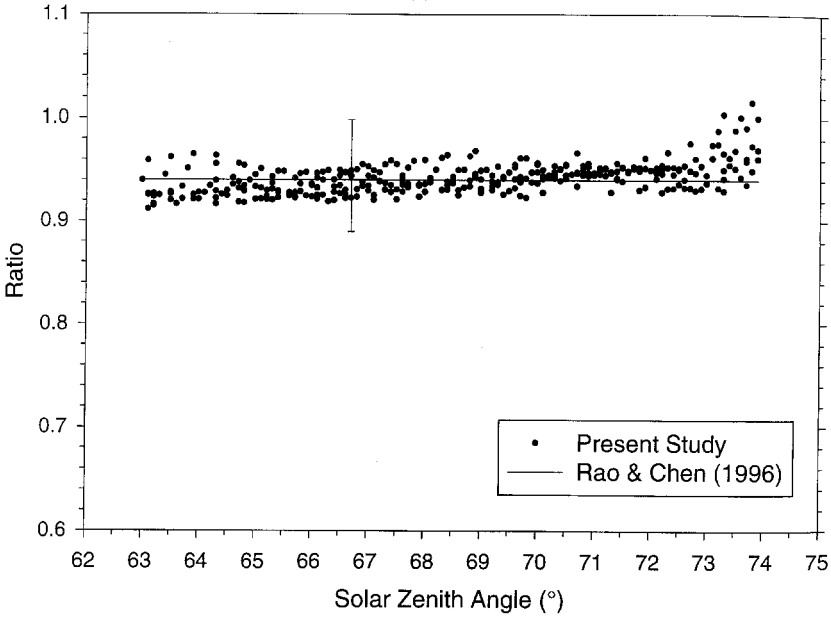

(*d*)

In figures 3 to 5, calibration coefficients inferred over Greenland and Antarctica are largely independent of θ_0. This implies that the NOAA-9 calibration reflectance curves provide a consistent description of the θ_0 dependence over these regions. Consequently, the present technique can be implemented with measurements over a small range of solar zenith angles. That is, it is not strictly necessary to use

Table 3. Calibration results for NOAA-11 based on the method described in the present study and from the formulae of Rao and Chen (1995). Absolute uncertainty for each coefficient is provided in parentheses.

		Channel 1			Channel 2		
Calibration	Date	α_1'	a_1'	γ_1	α_2'	a_2'	γ_2
Present study	June 1994	0·111 (0·005)	0·57 (0·03)	0·86 (0·04)	0·112 (0·007)	0·37 (0·02)	0·81 (0·05)
RC 1995	June 1994	0·114	0·59	0·84	0·123	0·41	0·73

Table 4. Calibration results for NOAA-14 based on the method described in the present study and from the formulae of Rao and Chen (1996). Absolute uncertainty for each coefficient is provided in parentheses.

		Channel 1			Channel 2		
Calibration	Date	α_1'	a_1'	γ_1	α_2'	a_2'	γ_2
Present study	June 1995	0·115 (0·005)	0·60 (0·03)	0·97 (0·04)	0·141 (0·008)	0·46 (0·03)	0·95 (0·05)
Present study	December 1995	0·118 (0·006)	0·61 (0·03)	0·95 (0·05)	0·142 (0·008)	0·47 (0·03)	0·94 (0·05)
Rao 1996	June 1995	0·113	0·59	0·99	0·136	0·45	0·99
Rao 1996	December 1995	0·117	0·61	0·95	0·142	0·48	0·94

(Note: γ_i were determined using the α_i values which appear on AVHRR data tapes after July, 1995.)

measurements over the entire range of θ_0 shown in these figures. This, together with the high frequency of satellite passes over Greenland and Antarctica, makes the method more flexible than those over desert regions. In the latter case, satellite passes are much less frequent (once per day), and there can be severe restrictions on the time of year (or day) in which calibration is possible due to vegetation cover, water vapour and aerosol abundance. Over Antarctica and Greenland, the effects of spatial variations in water vapour are likely to be small since temperatures there are so low. Similarly, since these regions are remote and free of any dust outbreaks, changes in aerosol abundance likely has less of an influence on the calibration than over desert. The main temporal constraint over Greenland and Antarctica is that due to the availability of sunlight. Given their proximity to the poles, however, sunlight is available over at least one of these two regions any time of year.

Table 5 shows the calibration results for NOAA-12 over an eighteen month period between June 1994 and December 1995. Over this period, changes in calibration are shown to be small (less than the uncertainty in α_i'). Compared to the prelaunch calibration coefficients for NOAA-12, however, these results represent an increase in α_1 of $\approx$20 per cent and an increase in α_2 of $\approx$35 per cent.

5. Summary and conclusions

Provided clouds are not present, reflectances over the ice-sheets of Greenland and Antarctica are radiometrically stable. Reflectances over these regions remain constant from year to year, and are spatially uniform over vast areas away from

Table 5. Calibration results for NOAA-12 based on the method described in the present study. Absolute uncertainty for each coefficient is provided in parentheses.

		Channel 1			Channel 2		
Calibration	Date	α_1'	a_1'	γ_1	α_2'	a_2'	γ_2
Present study	June 1994	0·124 (0·006)	0·64 (0·03)	0·82 (0·04)	0·144 (0·009)	0·48 (0·03)	0·72 (0·04)
Present study	December 1994	0·120 (0·006)	0·62 (0·03)	0·85 (0·05)	0·137 (0·007)	0·46 (0·02)	0·75 (0·04)
Present study	June 1995	0·125 (0·006)	0·64 (0·03)	0·82 (0·04)	0·145 (0·009)	0·48 (0·03)	0·71 (0·04)
Present study	December 1995	0·122 (0·007)	0·62 (0·03)	0·84 (0·05)	0·140 (0·008)	0·47 (0·03)	0·74 (0·04)

coastlines. Consequently, the interiors of Greenland and Antarctica serve as excellent calibration targets.

A new method for in-flight calibration of the visible and near-infrared channels of NOAA AVHRR radiometers has been described. Spatially uniform near-nadir NOAA-9 AVHRR reflectances over Greenland and Antarctica were used to produce reflectance calibration curves for calibrating AVHRR in other orbits. The calibration curves consist of second order polynomial regressions of reflectance on solar zenith angle. By comparing reflectances from an uncalibrated instrument with the calibration curves at the appropriate solar zenith angle, new channel 1 and 2 calibration coefficients are inferred with an accuracy of ≈5 per cent. The method is attractive since calibration targets over Greenland and Antarctica are very large; they are permanent, allowing calibration over multiple years; satellite passes are frequent over these regions; sensitivity to variations in water vapour and aerosol is smaller than over desert regions.

When calibration coefficients inferred over Greenland and Antarctica are compared with results from the Rao and Chen (1995, 1996) formulae for NOAA-11 (June 1994) and NOAA-14 (December 1994–95), the two methods are in excellent agreement in channel 1, with relative differences of less than 3 per cent. In channel 2, consistent results are obtained for NOAA-14, but significant differences are observed for NOAA-11. When the method is applied to NOAA-12 AVHRR measurements for 1994–95, channels 1 and 2 calibration coefficients are observed to be ≈20 per cent and ≈35 per cent larger than prelaunch values, respectively.

In conclusion, it is recommended that the present method be used to calibrate the AVHRR instruments in morning orbits (e.g., NOAA-10 and NOAA-12), for which no post-launch calibration is available. The method can also be used in comparisons with post-launch calibration results from desert regions for the afternoon orbits (e.g., NOAA-11, NOAA-14), and with future satellite instruments lacking on-board calibration.

Acknowledgments

The author would like to thank Professor J. A. Coakley, Jr. for his helpful comments and suggestions, and Dr. Nagaraja Rao for his suggestions and for making his calibration formulae readily available on the World Wide Web. This research was supported by NASA grant NAG 11263.

References

KAUFMAN, Y. J., and HOLBEN, B. N., 1993, Calibration of the AVHRR visible and near-IR bands by atmospheric scattering, ocean glint, and desert reflection. *International Journal of Remote Sensing,* **14,** 21–52.

KIDWELL, K. B., 1994, *NOAA Polar Orbiter Data Users Guide* (Washington, D.C.: U.S. Department of Commerce, National Oceanic and Atmospheric Administration, National Environmental Satellite, Data, and Information Service, National Climatic Data Center, Satellite Data Services Division).

RAO, C. R. N., and CHEN, J., 1995, Inter-satellite calibration linkages for the visible and near-infrared channels of the Advanced Very High Resolution Radiometer on the NOAA-7, -9, and -11 spacecraft. *International Journal of Remote Sensing*, **16,** 1931–1942.

RAO, C. R. N., and CHEN, J., 1996, Post-launch calibration of the visible and near-infrared channels of the Advanced Very High Resolution Radiometer on NOAA-14 spacecraft. *International Journal of Remote Sensing*, **17,** 2743–2747.

SMITH, G. R., LEVIN, R. H., ABEL, P., JACOBOWITZ, H., 1988, Calibration of the solar bands of the NOAA-9 AVHRR using high altitude aircraft measurements. *Journal of Atmosphere and Ocean*, **5,** 631–639.

STAYLOR, W. F., 1990, Degradation rate of the AVHRR visible channel for the NOAA-6, -7, and -9 spacecraft. *Journal of Atmospheric and Oceanic Technology*, **7,** 411–423.

TEILLET, P. M., SLATER, P. N., DING, Y., SANTER, R. P., JACKSON, R. D., and MORAN, M. S., 1990, Three methods for the absolute calibration of the NOAA AVHRR sensors in-flight. *Remote Sensing of Environment*, **31,** 105–120.

WARREN, S. G., and WISCOMBE, W. J., 1980, A model for the spectral albedo of snow: II: Snow containing atmospheric aerosols. *Journal of the Atmospheric Sciences*, **37,** 2734–2745.

WHITLOCK, C. H., STAYLOR, W. F., SUTTLES, J. T., SMITH, G., LEVIN, R., FROUIN, R., GAUTIER, C., TEILLET, P. M., SLATER, P. N., KAUFMAN, Y. J., HOLBEN, B. N., ROSSOW, W. B., BREST, C., and LECROY, S. R., 1990, AVHRR and VISSR satellite instrument calibration results for both cirrus and marine stratocumulus IFO periods. In *FIRE Science Results 1988, NASA Conference Proceedings* CP 3083 (Washington, D.C.: NASA).

WISCOMBE, W. J., and WARREN, S. G., 1980, A model for the spectral albedo of snow. I: Pure snow. *Journal of the Atmospheric Sciences*, **37,** 2712–2733.